JOURNAL OF GEOPHYSICAL RESEARCH, VOL. 86, NO. B7, PAGES 6143-6154, JULY 10, 1981

Laboratory Convection Experiments: Effect of Lateral Cooling and Generation of Instabilities in the Horizontal Boundary Layers

H. C. NATAF, C. FROIDEVAUX, AND J. L. LEVRAT

Laboratoire de Géophysique et Géodynamique Interne, Université Paris Sud, 91405 Orsay, France

M. RABINOWICZ

Groupe de Recherche en Géodésie Spatiale, Centre National d'Etudes Spatiales, 31055 Toulouse Cedex, France

Convection experiments are carried out in a tank with two isothermal heat sinks: The top plate and one of the sidewalls. Heating is supplied either by an isothermal bottom plate or by generation within the fluid. This situation is similar to that of the earth's subcontinental mantle in the presence of a neighboring subducting oceanic lithosphere. There, the mantle material loses heat not only to the base of the continental lithosphere but also to the cold dipping oceanic slab. The thermal structure of the convective fluid is observed by a variety of techniques, including differential interferometry and strioscopy. Two parameters characterize the observations: the usual 'vertical' Rayleigh number and a newly defined 'lateral' Rayleigh number. The lateral cooling induces a large roll with axis parallel to the cold wall. The variation of its width relative to the values of the two Rayleigh numbers has been determined. An application to the earth's upper mantle would predict rolls 5 times wider than high. The circulation in the large roll remains two-dimensional for Rayleigh numbers up to about 3×10^4. Beyond this value, boundary layer instabilities are observed within the persisting large roll. Their period has been determined. The interferometric method is shown to be very useful for visualizing other time-dependent processes such as the growth of the induced large rolls. This growth is rapid enough to allow us to propose the existence of such large rolls in the earth and argue that their action could have led to continental break-up.

INTRODUCTION

It is now generally accepted that the motion of tectonic plates on the earth's surface is a manifestation of thermal convection in the mantle. The precise relationship between the observed surface displacements and the convective pattern at depth is still unknown. Many specific inputs bear upon the physics of this problem. Thus considerable attention has been paid to the role of phase transitions [*Vening Meinesz,* 1962; *Schubert et al.,* 1975; *Sung and Burns,* 1976], the dependence in temperature and pressure of the viscosity [*Torrance and Turcotte,* 1971; *Lliboutry,* 1974; *Froidevaux et al.,* 1977], or the influence of the distribution of heat sources [*Howard et al.,* 1970; *McKenzie et al.,* 1974]. These aspects are usually treated in two-dimensional numerical experiments. Laboratory experiments could be carried out in some cases. For example, the effect of temperature-dependent viscosity [*Booker,* 1976; *Richter,* 1978] and internal heating [*Tritton and Zarraga,* 1967; *De La Cruz,* 1970] has been studied.

Coupling between oceanic lithosphere and subcontinental convection. This paper focuses attention on one major feature: the influence of the sinking oceanic lithosphere on the neighboring subcontinental convection [*Rabinowicz et al.,* 1980]. This refers to the striking subdivision of the earth's surface into two domains: continents and oceans. Because of the low density of its crust, the continental lithosphere does not take part in the convective circulation. On the contrary, the oceanic lithosphere is an active part of mantle convection: it is created at ridges, cools and thickens as it moves toward the trenches, where it sinks back into the mantle. Therefore it can be considered as the upper thermal boundary layer of the suboceanic convection, the exchange of heat taking place at 0°C in contact with the sea water. This is illustrated in Figure 1. By contrast, the convective layer under continents exchanges heat in contact with the base of the lithosphere, i.e., at a temperature of the order of 1200°C. This temperature corresponds to the transition between the mechanically rigid lithospheric material and the softer asthenospheric material underneath it. Small scale sublithospheric convection might also exist under oceanic plates [*Richter and Parsons,* 1975; *McKenzie et al.,* 1980]. Its presence would not change the general picture we present here, as the cooling of the lithosphere is anyway the dominant factor in oceanic heat transfer. The oceanic lithosphere has reached a very low mean temperature at the time it sinks back into the mantle. The lower part of Figure 1 shows the thermal boundary conditions prevailing in the subcontinental asthenosphere in the presence of a neighboring subduction zone. Schematically, they can be described by means of an upper cold isothermal plate and an even colder sidewall. The heat input may be provided partly through the bottom and partly within the fluid or it may simply be imposed by a hot isothermal lower boundary, say at 2000°C if a depth of 700 km is chosen. The choice of depth scale constitutes one of today's open problems [*Davies,* 1977; *Richter,* 1979; *Allègre,* 1980]. We shall see that these peculiar boundary conditions give rise to spectacular changes in the convective pattern.

Two-dimensional numerical models. The effect of lateral cooling of the continental asthenosphere by the subducting oceanic lithosphere has been studied numerically [*Rabinowicz et al.,* 1980]. The cooled material sinks down the sidewall and has to flow a long distance along the lower boundary before it absorbs enough heat to become buoyant and rise. Thus a wide roll with axis parallel to the cold wall characterizes the steady state as illustrated in the lower part of Figure 1. These numer-

Paper number 1B0369.
0148-0227/81/001B-0369$01.00

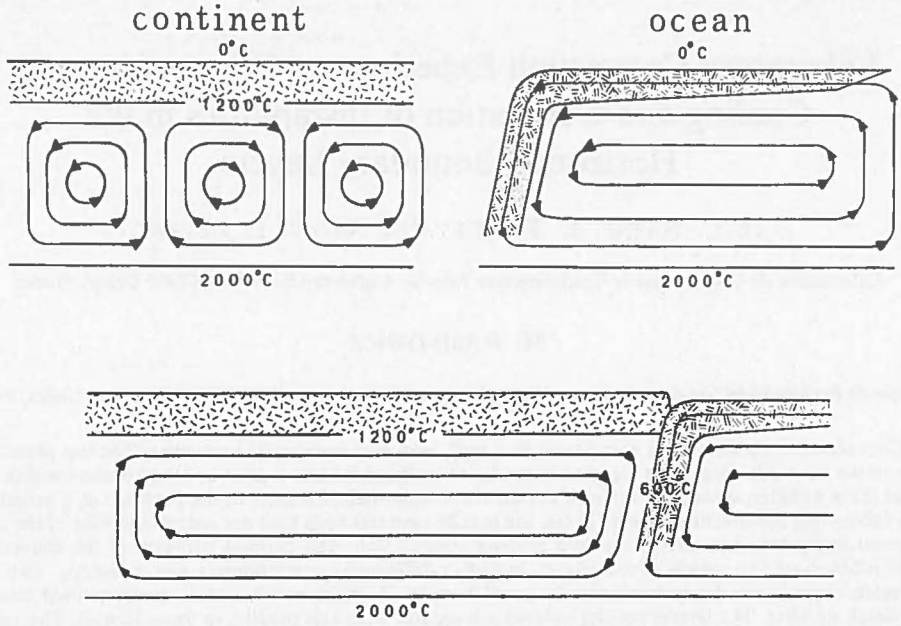

Fig. 1. Sketch of the convective circulation in the upper mantle underneath continents and oceans. At the top, the two systems are considered separately. The rigidity of the lithosphere (shaded area) is assumed to impose a large scale flow under oceans. The lower diagram is an idealized view of the interaction between both domains. It shows, in particular, that the convective mantle under the continental lithosphere is confined by three boundaries having very different mean temperatures. Thus two heat sinks are now present, the one on the side being much cooler than the top one.

ical models are claimed to be geophysically relevant. The lateral transfer of heat explains the low observed value of the reduced heat flow under continents compared to the mean oceanic value. The wide roll exerts a drag under the continental lithosphere. Combined with the thermal effect of the upwelling limb, it may generate rifting. Baikal is a candidate for such a mechanism, if subduction in the West Pacific induces a wide roll under Asia. This proposal is supported by the presence of a long wavelength anomaly in the geoid (3000 km). The gravity signal observed is precisely the one predicted by the wide roll model [*Rabinowicz,* 1980].

Usefulness of laboratory models. The physical validity of the two-dimensional steady state numerical experiments can be checked by carrying out properly scaled laboratory experiments. One can thereby explore three-dimensional behavior as well as time-dependent structures. This requirement provided the initial motivation for the present work. Laboratory experiments cannot cope with all the complexities of mantle convection. They are best performed in order to deepen our physical insight of some well-defined aspects. Here, we study two simple cases of lateral cooling: (1) convection driven by three isothermal plates, i.e., Rayleigh-Bénard configuration with an additional cold sidewall and (2) convection of an internally heated fluid cooled by two isothermal plates, the lateral one being colder than the top one. These situations are shown in Figure 2. So far, no attention seems to have been paid to these simple boundary conditions involving a double heat sink. An exception is the treatment of convection driven by two vertical isothermal plates in very elongated cavities with some weak heat loss through the upper surface [*Cormack et al.,* 1975]. Our first experimental results confirm the existence of the wide convective roll induced by lateral cooling, illustrate its growth versus time, and explore its three-dimensional structure. Two Rayleigh numbers, one vertical and one lateral, are shown to characterize the flow, in particular the width of the large roll and the occurrence of boundary layer instabilities within it. The observation of these phenomena was achieved by means of the combination of several optical techniques including differential interferometry.

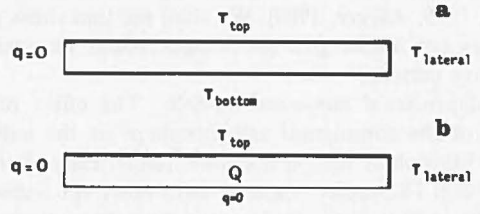

Fig. 2. Two sets of thermal boundary conditions for the experiments. (*a*) Three isothermal plates, the other sidewalls being insulating; (*b*) two isothermal heat sinks and internal heat generation Q; no heat flow through the bottom plate and other sidewalls.

EXPERIMENTAL PROCEDURE

The tank. Figure 3 shows the experimental tank. The top copper plate is maintained at a given temperature T_{top} by a circulating fluid and insulated from the environment by a plexiglass cover. The fluid is confined inside the central transparent plexiglass frame. The latter is adequate for observations by means of optical methods and provides good thermal insulation. One short side of this central frame is a cooled copper plate at temperature $T_{lateral}$. A thin plexiglass sheet insulates it from the top plate. The bottom plate can be identical to the top one in order to impose a chosen temperature T_{bottom}. In the figure, it consists of an insulating plexiglass plate coated with a semitransparent gold film. This last configuration is used for internal heating, which is achieved by passing an electrical current between the gold film and the top copper plate across the fluid. Thermocouples are imbeded in narrow holes inside the copper plates to monitor temperature differ-

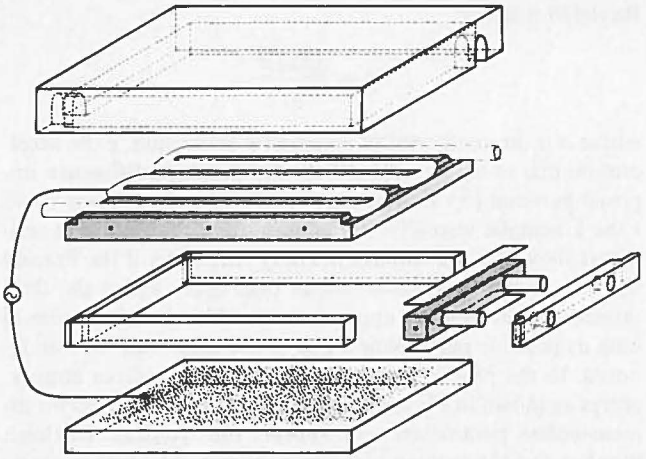

Fig. 3. Elements of the experimental tank. The convecting fluid is confined in the middle frame with the cooled sidewall on the right. Its inner dimensions are: depth (2 ± 0.01) cm, base (10 ± 0.1) × (20 ± 0.1) cm. The horizontal position of the tank is achieved with a ±0.5 mm/m accuracy. Dark shading indicates copper, and light shading a gold deposit 0.150 μm thick. The copper tubing is not shaded. Transparent elements are made of plexiglass. The position of holes for chromel-alumel thermocouples is indicated. Temperature differences between plates are set between 1° and 30°C and are stable within ±1% over several hours. Temperature differences within one single plate are less than ±4% of the temperature difference between plates. The alternative current crossing the fluid dissipates up to 22 W when driven by 150 V. This tank is similar to the Rayleigh-Bénard set-up used by *Dubois and Bergé* [1978].

ences, either within one plate or between two plates. Silicon oils with Prandtl number 440, 1300, or 3100 (see Table 1 for detailed properties) have been used when the fluid is heated from below. Our experiments with internal heating used a mixture of glycerol and water containing KNO_3 as an electrolytic working fluid. The Prandtl numbers are 210 or 3900 (see Table 1). As the electrical conductivity is a function of temperature, some care has to be taken to minimize a possible coupling between the convection pattern and the nonuniformity of heating [*Schwiderski and Schwab,* 1971]. This coupling is strongest when the electric current flows horizontally in the fluid. This is why, like other workers [*De La Cruz,* 1970], we use the top and bottom plates as electrodes. In our experiments, the heat generation turns out to be twice as large at the top than at the bottom of the fluid. Although the copper sidewall is coated with varnish, we could not completely avoid the formation of gas bubbles on it when the 50 Hz alternating current flows through the fluid. This limits our working time to a few hours. With heating from below, the conditions are more favorable: the convection pattern can be observed over periods greatly exceeding the characteristic thermal time d^2/κ, which amounts to about 1 hour.

Optical methods. Extensive use was made of differential interferometry to observe the temperature structure of the convecting fluid. This method is based on the interference between pairs of light rays after they cross the fluid along slightly displaced parallel paths. The resulting fringes correspond to lines of constant temperature gradient [*Merzkirch,* 1974; *Oertel and Bühler,* 1978]. The optical method used here is very convenient because it is compensated even for large incident angles, so that a wide luminous source can be used [*Françon and Mallick,* 1971]. Figure 4 is a view of the tank from above. The light is split into two orthogonally polarized components after passing through the first optical device made of oriented quartz crystals. The recombination of the two components, which suffer a phase shift when passing through the fluid, takes place in an identical optical device, and a fringe pattern is formed on a screen or directly on a photographic film. If the split light rays are in a horizontal plane as in the figure, the fringes are lines of equal horizontal temperature gradient. If, on the contrary, they lie in a vertical plane, the fringes are lines of equal vertical gradient. Between two close fringes, dark or light, the temperature gradient varies by

$$\Delta\left(\frac{\partial T}{\partial x}\right) = \frac{\lambda}{el}\,\frac{6n_0}{(n_0^2+2)^2\rho_0\alpha R}$$

where e is the ray separation, λ the wavelength, l the path length through the tank, α the expansion coefficient of the fluid, ρ_0 and n_0 its reference density and refractive index. The constant R derives from the Lorentz-Lorenz formula $(n^2 - 1)/(n^2 + 2) = R\rho$, relating the refractive index to the density. It characterizes the fluid and varies with wavelength. For our ex-

TABLE 1. Properties of Working Fluids

	Silicon Oils 'Rhodorsil'			Glycerol + Water + KNO_3	
	47V350	47V150	47V50	96%	74%
Prandtl number	3100	1300	440	3900	210
Kinematic viscosity at 25°C (m^2/s)	3.5×10^{-4}	1.5×10^{-4}	0.5×10^{-4}	3.5×10^{-4}	0.21×10^{-4}
Density at 25°C (kg/m^3)	0.970×10^3	0.965×10^3	0.959×10^3	1.248×10^3	1.189×10^3
Expansion coefficient ($°C^{-1}$)	9.45×10^{-4}	10^{-3}	1.05×10^{-3}	4.9×10^{-4}	4.95×10^{-4}
Specific heat (J/kg/°C)	1.46×10^3	1.46×10^3	1.46×10^3	2.7×10^3	3×10^3
Thermal conductivity (W/m/°C)	0.16	0.16	0.16	0.3	0.36
Thermal diffusivity (m^2/s)	1.13×10^{-7}	1.13×10^{-7}	1.14×10^{-7}	0.9×10^{-7}	10^{-7}
Weight percentage in glycerol				96	74
Concentration in KNO_3 (g/l)				1.1	0.07
Electric conductivity at 25°C ($\Omega^{-1}\,m^{-1}$)				6×10^{-4}	6.4×10^{-4}
Refractive index at 25°C (Na line D)	1.403	1.403	1.402	1.47	1.44
Thermal diffusion time d^2/κ (s)	3540	3540	3510	4400	4000
Interfringe (°C/cm)	2.4	2.3	2.2	3.9	4.1

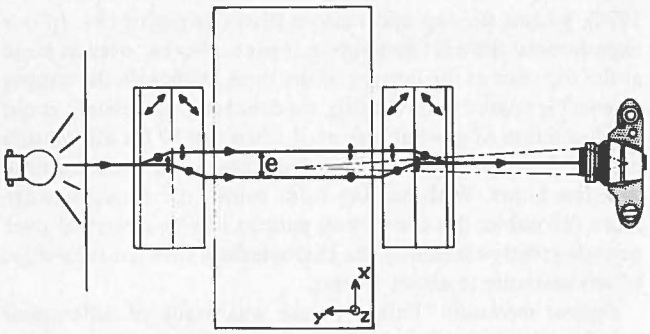

Fig. 4. Plan view of the differential interferometry set-up. The optical devices on each side of the tank are cylindrical with diameter 7 cm. Each quartz crystal is 1 cm thick, the arrows indicating their optical axis. They are separated by a $\lambda/2$ film. The third layer is a polarizer with axis at 45° with the plane of the figure. The split rays are polarized as indicated, and their distance e amounts to 58 μm. The various elements of this drawing are not to scale.

periments with silicon oils, one gets $\Delta(\partial T/\partial x)$ values around 2.4°C/cm.

Whereas the above method yields an instantaneous complete sideview of the convective thermal structure, strioscopy provides the value of the mean temperature gradient along a single path. Its principle sketched in Figure 5 is based on the deflection of a narrow beam by the variation of the refractive index in the plane normal to the path. The deflection angle i relates to the temperature gradient by

$$i = -\frac{R\rho_0\alpha(n_0^2+2)^2}{6n_0}\frac{\partial T}{\partial x}$$

In practice, the laser beam crossing the tank is focused by a cylindrical lens on an optical recorder. Horizontal (vertical) temperature gradients are monitored when the lens axis is horizontal (vertical). The method is sensitive and was found useful for investigating local time-dependent behavior or measuring the heat flux at boundaries.

Other more conventional techniques have been combined with the above methods. Aluminum flakes suspended in the fluid trace trajectories in long-exposure photographs. They yield a streamline pattern of the steady state and a rough estimate of the velocity field in any chosen section of the tank which is illuminated. Finally, use was made of the shadowgraph technique [*Chen and Whitehead,* 1968] to obtain a global picture of the convection planform. This method is based on the focusing (defocusing) action of cold (hot) columns of fluid on a light beam crossing the tank vertically. This could only be introduced in the tank with internal heating. In that case, the lower plate is indeed semitransparent, being made of plexiglass coated with a thin gold deposit which acts as an electrode. The top copper plate is polished to form a reflecting mirror.

RESULTS

A large number of convection experiments have been performed. They first aimed at determinating appropriate dimensionless parameters, so that general conclusions may be drawn. A quantitative comparison with numerical two-dimensional models was then attempted. Finally, time-dependent phenomena were investigated in some detail.

Dimensionless parameters. The onset of Rayleigh-Bénard convection in a fluid layer of thickness d is known to depend upon the value of a single dimensionless quantity, the Rayleigh number:

$$Ra = \frac{\alpha g \Delta T d^3}{\kappa\nu}$$

where α is the coefficient of volumetric expansion, g the acceleration due to the gravity, ΔT the temperature difference imposed between top and bottom, κ the thermal diffusivity, and ν the kinematic viscosity. Finite amplitude convection experiments show that Ra remains the only parameter if the Prandtl number $Pr = \nu/\kappa$ is much greater than unity and if the fluid satisfies the Boussinesq approximation. This is strictly true as long as possible perturbation due to the tank walls can be ignored. In the problem of convection driven by three temperatures as shown in Figure 2*a*, one naturally thinks that two dimensionless parameters will appear: the 'vertical' Rayleigh number and the temperature contrast ratio. The first quantity Ra_{vertical} is the usual Rayleigh number with the temperature difference $\Delta T = T_{\text{bottom}} - T_{\text{top}}$. The temperature contrast ratio on the other hand is defined as:

$$c = \frac{T_{\text{bottom}} - T_{\text{lateral}}}{T_{\text{bottom}} - T_{\text{top}}}$$

One may approach the problem differently by noticing that convection along an infinite vertical cold plate in an isothermal environment depends on a local Rayleigh number $Ra_z = \alpha g \Delta T z^3/\kappa\nu$, where z represents the distance from the leading edge (top) of the cold plate [*Holman,* 1976]. A thermal boundary layer forms along the cold plate. Its thickness δ is given by $\delta = 1.1z(Ra_z)^{-1/4}$. The maximum velocity is $u = 0.77(\kappa/z)(Ra_z)^{1/2}$. These results are for $Pr \gg 1$ [*Holman,* 1976]. In our problem, the maximum z is the depth of the tank d. It corresponds to the height of the cold sidewall. We thus define a 'lateral' Rayleigh number:

$$Ra_{\text{lateral}} = \frac{\alpha g(T_{\text{bottom}} - T_{\text{lateral}})d^3}{\kappa\nu}$$

It characterizes the driving capability of the lateral cold boundary layer. For convection driven by two vertical isothermal walls [*Gill,* 1966], we find that Ra_{lateral} is the relevant dimensionless parameter when Pr and Ra are large. This follows if one takes κ/d for the unit velocity as in the Rayleigh-Bénard case. For convection driven by three temperatures, we shall attempt to use the two Rayleigh numbers Ra_{vertical} and Ra_{lateral}. The use of Ra_{lateral} is more general than the use of c, as it can include the cases $Ra_{\text{vertical}} = 0$ (for which $c = \infty$). One has $Ra_{\text{lateral}} = cRa_{\text{vertical}}$.

For convection experiments with internal heating the Rayleigh number can be defined as follows [*Roberts,* 1967]:

$$Ra^* = \frac{\alpha g Q d^5}{k\kappa\nu}$$

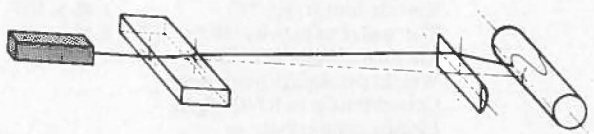

Fig. 5. Schematic set-up for strioscopy. The light beam emitted by a laser crosses the tank, where it is deflected. A cylindrical lense focuses the beam on the horizontal slot of an optical recorder. The axis of the last two elements can be set vertically in order to record the vertical, rather than horizontal, component of the deflection. The latter is exaggerated on the drawing where the various elements are not to scale.

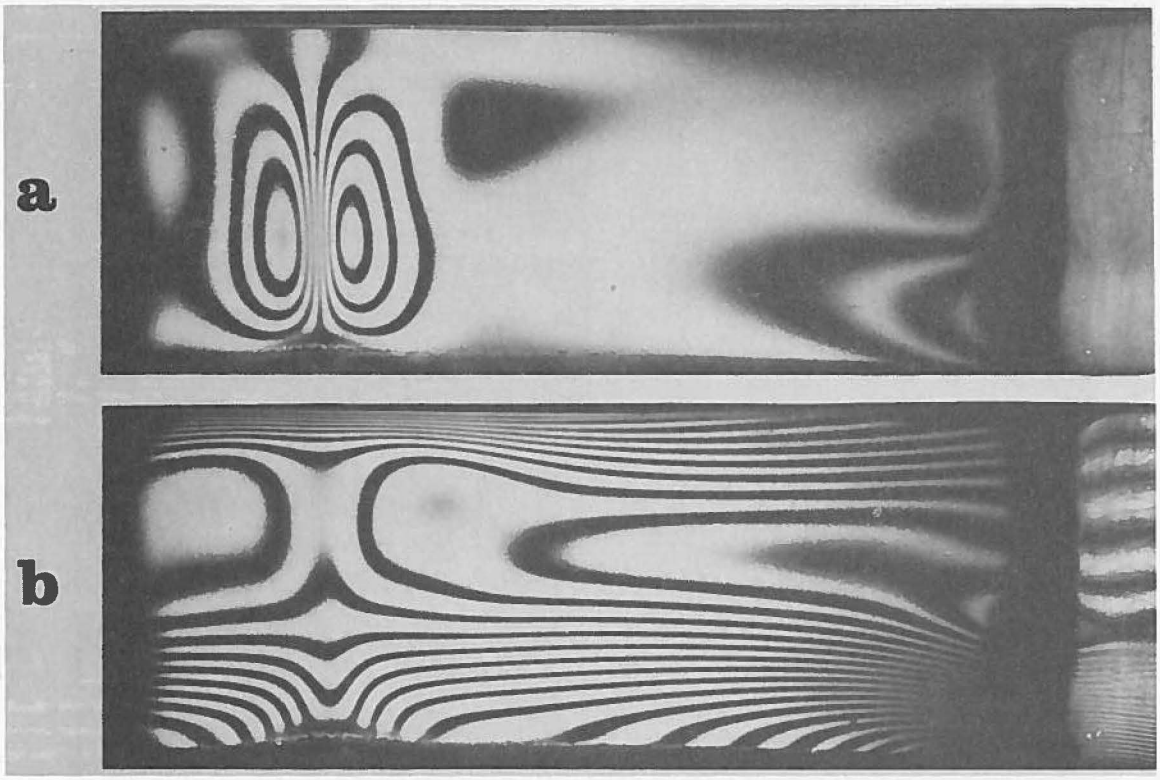

Fig. 6. Differential interferometry pattern of a portion of the tank next to the cold sidewall on the right. A large roll and a fragment of the next square roll are visible. The fringes are lines of constant (*a*) horizontal and (*b*) vertical temperature gradients. The conditions are: $Ra_{vertical} = 30{,}000$; $Ra_{lateral} = 44{,}000$; $Pr = 3100$. Between two dark fringes, the temperature gradient varies by 2.45°C/cm. The pattern is deformed by the deflection of the light crossing regions with high gradients. This causes a noticeable asymmetry in the apparent thickness of the upper and lower boundary layers. The lateral boundary layer is not fully resolved in Figure 6*a*, as it falls outside the interferometry field.

Here Q is the volumetric rate of heat generation and k the thermal conductivity. The definition of two equivalent numbers when lateral cooling is added, i.e., for the case pictured in Figure 2*b*, will not be attempted here. The convective behavior of the fluid far from the cold wall is described by means of the heat production, which is the relevant external parameter. On the other hand, the temperature of the lateral boundary is externally imposed. The number of runs performed with internal heating is insufficient to allow us to make a choice among the various dimensionless $Ra_{lateral}$ one can think of.

The most striking feature of the convection pattern in the presence of lateral cooling is the formation of a wide roll with axis parallel to the cold wall. Figure 6 shows the part of the tank next to the cold wall which is on the right-hand side of the photographs. These differential interferometry patterns show the same wide roll by means of both the horizontal and vertical temperature isogradients. The convection cells in the remaining part of the tank are standard cross rolls with aspect ratio close to unity. They are outside of the field of the photographs. Let us see how the size of this large roll varies with the parameters $Ra_{vertical}$ and $Ra_{lateral}$ defined above. Figure 7 plots the value of the width over depth ratio w/d in terms of these two parameters. For a fixed value of $Ra_{vertical}$ the size of the roll increases with increasing $Ra_{lateral}$. For a fixed value of $Ra_{lateral}$, on the other hand, it decreases with increasing $Ra_{vertical}$. Although three fluids with different Prandtl numbers were used, the data points for $Ra_{vertical} = 3 \times 10^4$ and $Ra_{vertical} = 0$ are seen to fall on single straight lines. This illustrates the absence of variation with Pr. The plot also demonstrates the validity of the chosen Rayleigh numbers to define the physical

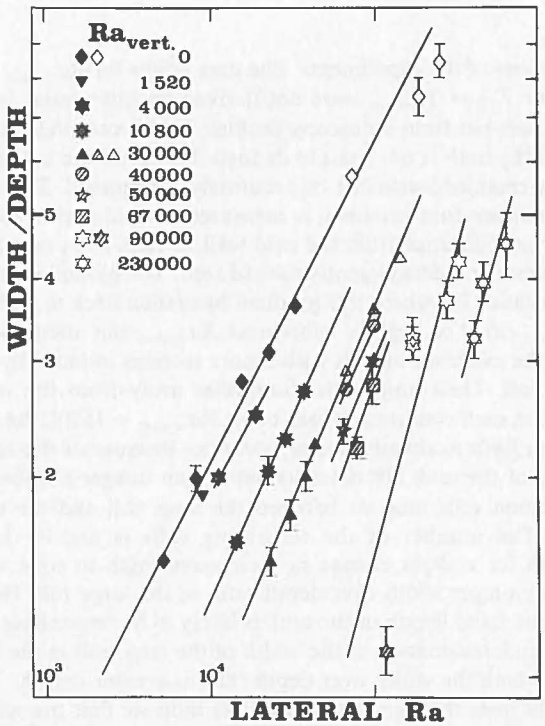

Fig. 7. Width over depth ratio of the large roll versus lateral Rayleigh number. Each type of symbol corresponds to a given value of $Ra_{vertical}$ listed in the top left corner. Solid symbols are for Prandtl number value $Pr = 3100$, shaded symbols for $Pr = 1300$, and open symbols for $Pr = 440$. Straight lines are drawn through the data points with identical $Ra_{vertical}$ values.

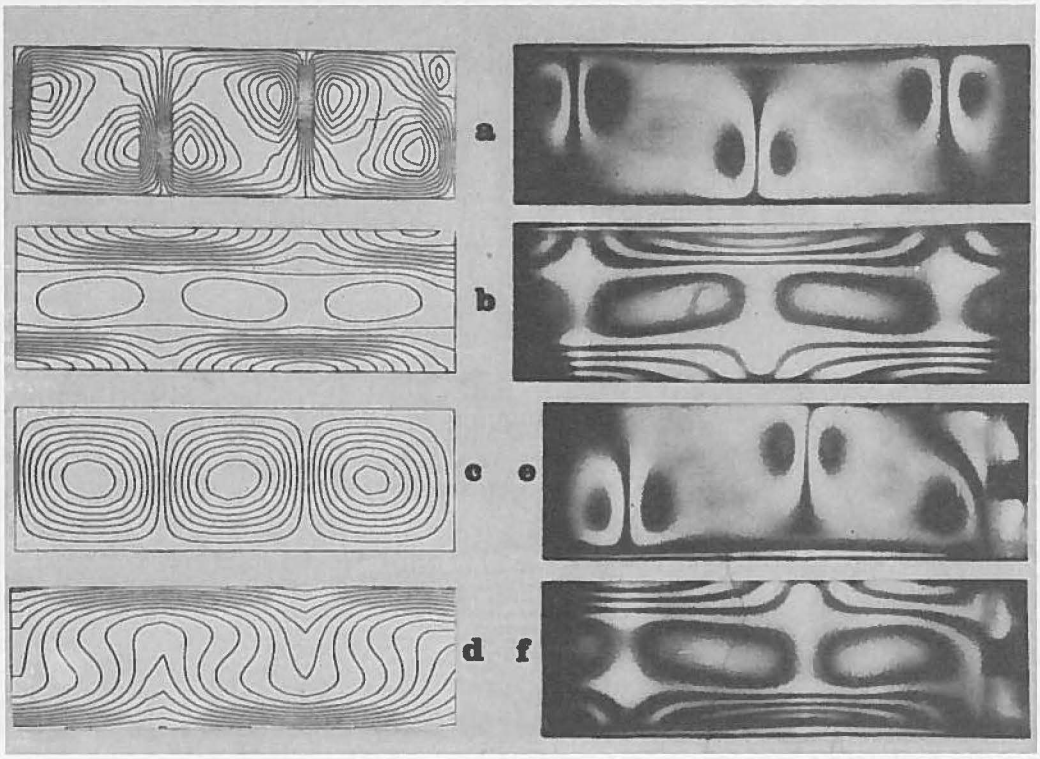

Fig. 8. Computed and experimental solutions for Rayleigh-Bénard convection. The same parameters are used for both cases: $T_{top} = 22.1°C$, $T_{bottom} = 27.9°C$, $Ra = 10{,}900$, silicon oil with $Pr = 3100$ in the experiment but infinite Pr for the computations. The frames illustrate (*a*) the horizontal isogradients, (*b*) the vertical isogradients, (*c*) the computed stream lines, (*d*) the computed isotherms, and (*e* and *f*) a detail related with the presence of an insulating wall also found in the computed solutions in Figures 8*a* and 8*b*. The experimental frames (Figures 8*a* and 8*b*) show a portion of the middle part of the tank. The interfringe values differ in the computed and experimental solutions so that the number of fringes is not identical.

conditions of the experiments. The data points for $Ra_{vertical} = 0$, i.e., for $T_{top} = T_{bottom}$, were not derived by differential interferometry but from strioscopy profiles. In this case indeed the upwelling limb is not sharply defined. However, the extent of the thermal influence can be accurately determined. The vertical temperature gradient is measured at mid-depth versus horizontal distance from the cold wall. It rises from zero to a maximum and decays gently toward zero. The plotted width is the distance for which this gradient has fallen back to $0.5\% \times (\Delta T_{lateral}/d)$. For slightly subcritical $Ra_{vertical}$ this method reveals the existence of rolls with square sections induced by the large roll. Their amplitude diminishes away from the large roll. For such conditions (data point $Ra_{vertical} = 1520$), the upwelling limb is already sharply defined. Because of the finite length of the tank (10 times its depth), an integer number of convection cells must fit between the large roll and the endwall. The number of the remaining cells is usually large enough for a slight change in their wavelength to cope with the noninteger width over depth ratio of the large roll. However, the finite length of the tank is likely to be responsible for some underestimation of the width of the large roll in the two cases where the width over depth ratio is greater than 8. The straight lines through the data points indicate that the width of the large roll is roughly proportional to $(Ra_{lateral})^{1/2}$. The $Ra_{vertical}$ dependence is weaker, something like $(Ra_{vertical})^{-1/3}$. It follows that, at constant temperature ratio c, the width of the large roll is about proportional to $(Ra_{vertical})^{1/6}$. For example for $c = 2$ and $Ra_{vertical} = 10^4$, the large roll is twice wider than deep. For the same temperature contrast ratio, but for $Ra_{vertical} = 10^6$, the induced roll becomes 5 times wider than deep.

A limited number of experiments with internal heating have been carried out. They exhibit large rolls with width/depth ratios between 4 and 10 and will be discussed when other aspects of the convective pattern will be presented.

Comparison with numerical experiments. Having analyzed the global dimension of the induced large roll, which represents the most apparent feature and is very sensitive to imposed conditions, let us consider its thermal and mechanical structure in more detail. In particular, let us compare the results of differential interferometry and the use of tracers with numerical computations. The computations are for low Rayleigh numbers. They are based on a finite difference scheme described elsewhere [*Rabinowicz et al.*, 1980]. Figure 8 illustrates the results for Rayleigh-Bénard convection without lateral cooling for $Ra = 10{,}900$. The computed and observed isogradient patterns exhibit identical general features. In Figure 8*a* the lines of constant horizontal temperature gradient concentrate around the base of the uprising and the top of the downwelling currents. The number of fringes between the numerical and the laboratory patterns differ because the chosen values of $\Delta(\partial T/\partial x)$ are not the same. The square rolls are

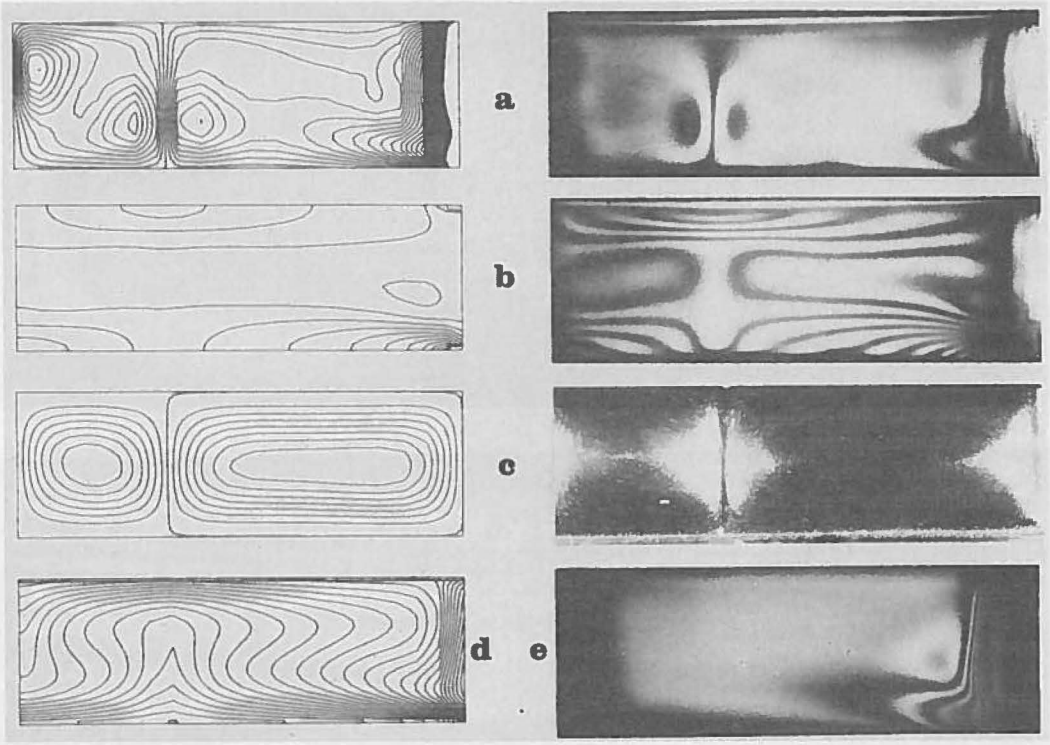

Fig. 9. Computed and experimental solutions for convection with three isothermal boundaries. $T_{top} = 22.1°C$, $T_{bottom} = 27.9°C$, and $T_{lateral} = 17°C$. This yields $Ra_{vertical} = 10{,}900$ and $Ra_{lateral} = 20{,}400$, other conditions being as in Figure 8. The cold sidewall lies on the right-hand side of each frame. (*a*) Horizontal isogradients, (*b*) vertical isogradients, (*c*) streamlines, and (*d*) isotherms. The exposure for the experimental streamlines lasted 8.0 s. (*e*) Details of the horizontal isogradients near the cold wall for an experiment with $Ra_{vertical} = 31{,}000$, $Ra_{lateral} = 67{,}500$, and $Pr = 1300$.

separated by a vertical fringe corresponding to $\partial T/\partial x = 0$. In Figure 8*b* the computed and observed fringes of constant vertical temperature gradient $\partial T/\partial z$ also show good agreement. A large number of fringes characterize the upper and lower thermal boundary layers. The computed streamlines and isotherms are pictured in Figures 8*c* and 8*d*. The figure contains two more interferometry pictures (Figures 8*e* and 8*f*) illustrating the perturbation introduced by the presence of an insulating sidewall on the right-hand side. This effect is also present in the computed patterns, which have also a right-hand wall with no slip and no heat input. For the left-hand wall, symmetry is assumed. The excellent agreement between numerical and laboratory experiments is further demonstrated in this particular sensitive detail. The isogradient pattern turns out to be highly performant.

Figure 9 illustrates the case with lateral cooling. The values of the Rayleigh numbers are $Ra_{vertical} = 10{,}900$ and $Ra_{lateral} = 20{,}400$. A large roll forms next to the cold wall while the other rolls remain unchanged. In the experiment, the flow is still bidimensional. The horizontal isogradients (Figure 9*a*) reveal the formation of a thermal boundary layer next to the cold wall. Figure 9*e* gives a better view of this region of the tank for a case where the number of fringes is greater since the Rayleigh numbers are higher. In the upper part of this picture the high number of fringes in the thickening thermal boundary indicates a high lateral heat flow. Further down, the fringes bend toward the cold wall. Their decreasing number corresponds to a lower lateral heat loss as the flow of cooled material turns parallel to the bottom plate. There the cold tongue is strongly heated and the vertical isogradients in Figure 9*b* show the formation of a horizontal boundary layer. Ultimately, the material becomes buoyant again and rises. This can also be seen by observing the streamlines revealed by tracer particles in Figure 9*c*. In Figure 9*d* the computed pattern of isotherms is given. Table 2 shows that a quantitative agreement is found for the main characteristics of the flow.

It is interesting to look now at the thermal structure of the large roll for the case of internal heating. Figure 10 shows both the horizontal and the vertical isogradients. The striking difference from the previous figures is the absence of a bottom thermal boundary layer in Figure 10*b*. This was of course ex-

TABLE 2. Comparison Between Numerical and Laboratory Experiments

	Numerical	Laboratory
Width/Depth	2	2.1
Maximum velocity (mm/s)		
Downwelling	0.17	0.17 ± 0.02
Uprising	0.20	0.21 ± 0.02
Mean heat flux (W/m²)		
Lateral wall	275	> 100
Bottom	205	200 ± 20
Top	68	80 ± 10

Velocities and heat flux values are derived for the large roll shown in Figure 9. The experimental values of the maximum velocity in the downwelling and uprising currents are deduced from the length of the strikes on the long exposure picture. The isogradient fringes next to the boundaries are used to determine the local heat flux.

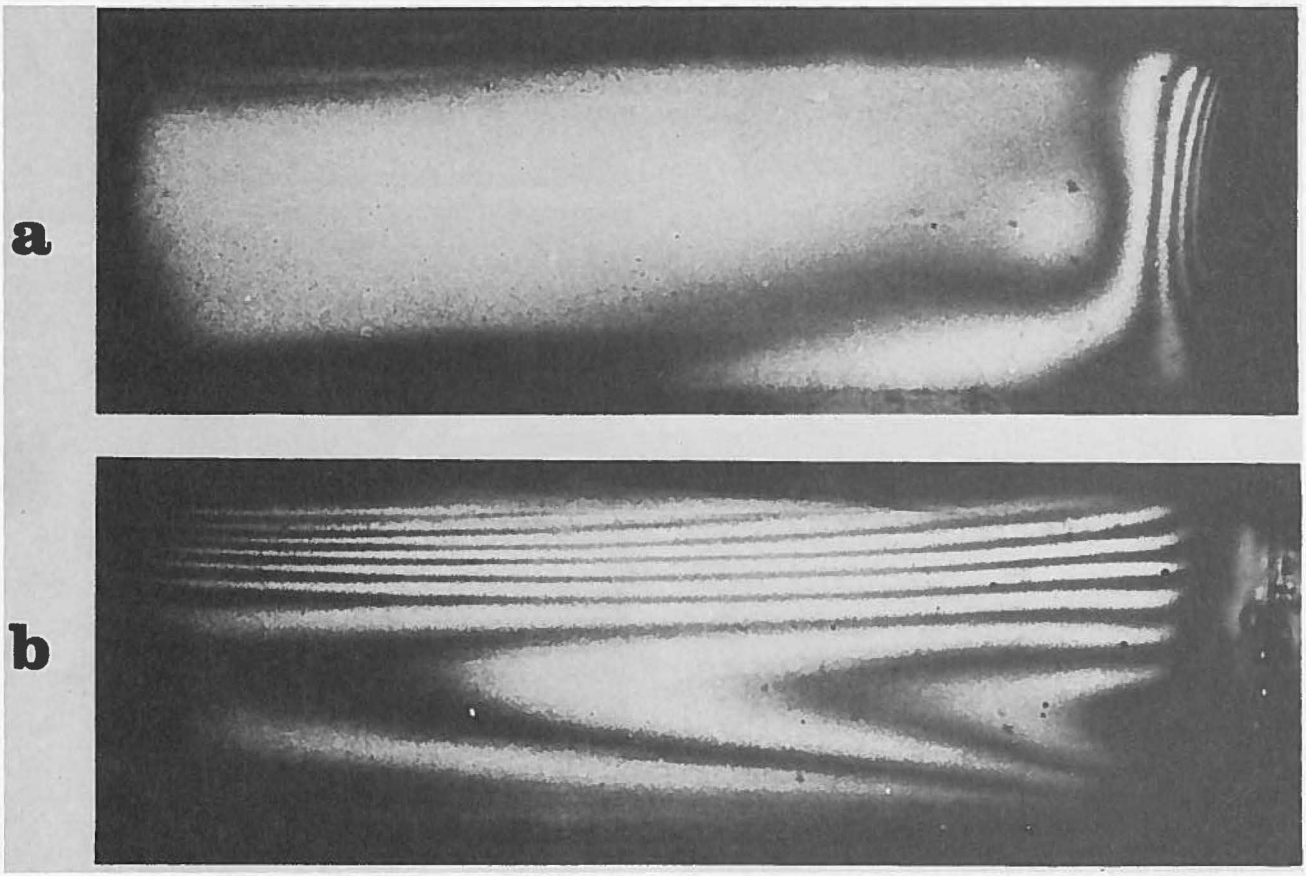

Fig. 10. Differential interferometry pictures for convection with internal heating and two heat sinks. Conditions are: $T_{top} = 20°C$, $T_{lateral} = 10.9°C$, $Q = 55$ kW/m^3, $Ra_{vertical}^* = 140{,}000$ and $Pr = 3900$. The (*a*) horizontal and (*b*) vertical isogradient fringes show a portion only of a large roll with $w/d = 4$ next to the cold sidewall. For internal heating the working fluid gives a different value of the interfringe, here about 4°C/cm.

pected, as the lower boundary is now insulating. Here the cold wall is again on the right-hand side, but the other extremity of the large roll is located outside of the picture.

Instabilities in the thermal boundary layers. For larger Rayleigh numbers, the circulation within the large roll exhibits time-dependent features. This can be seen in Figure 11, which corresponds to $Ra_{vertical} = 67{,}000$ and $Ra_{lateral} = 97{,}000$. Undulations appear in the fringe pattern of the lower thermal boundary layer (Figure 11*b*). They correspond to the formation of hot ascending plumes which have a characteristic signature in the horizontal isogradient picture (Figure 11*a*). This small scale motion could also be observed with the help of tracers. The plumes originate on the lower plate at some distance from the cold sidewall and are carried away by the persisting large scale circulation. Thus the thermal structure in the left-hand portion of the large roll swings to the left in the lower part and to the right in the upper part. In usual Rayleigh-Bénard convection, the thickness of the boundary layers diminishes when the Rayleigh number increases. This trend can also be observed here by comparing Figures 9*b* and 11*b*. Although the thickness is reduced, the temperature drop across the thermal boundary layer is increased for high Rayleigh numbers. Thus the boundary layer itself becomes unstable. This can be expected to happen at some distance from the cold wall where the thickness becomes large enough for the local Rayleigh number to be critical. The interferometry patterns illustrate this thickening. The temperature fluctuations connected with the generation of the instabilities can be recorded by strioscopy. Figure 12 shows the horizontal deflection of the light beam versus time. It reflects quasi-periodic variations in the mean temperature gradient along the path of the light beam within the unstable portion of the lower boundary layer. The variation of amplitude might be connected with the occurrence of several distinct plumes along the path, which is 5 times longer than the depth of the tank. However, no observations have been made to analyze this point. Figure 13 gives the measured period of these fluctuations versus vertical Rayleigh number for two different $Ra_{lateral}$ values. In the Rayleigh-Bénard case, the period is proportional to $(Ra_{vertical})^{-2/3}$ [*Bergé and Dubois,* 1979]. Our data points are compatible with such a variation but displaced to lower values. The bigger $Ra_{lateral}$, the bigger this displacement. The observed fluctuations are thought to be true boundary layer instabilities, independent of Prandtl number. They are not connected with oscillations of the spatial position of the convective cells observed for Rayleigh-Bénard convection in large tanks [*Busse and Whitehead,* 1974]. Here the cold wall stabilizes the position of the large roll so that the boundary layer effect alone is present, a situation somewhat similar to what occurs for Rayleigh-Bénard convection in 'small boxes' [*Bergé and Pomeau,* 1980]. Numerical models with infinite Prandtl number [*McKenzie et al.,* 1974; *Lux et al.,* 1979;

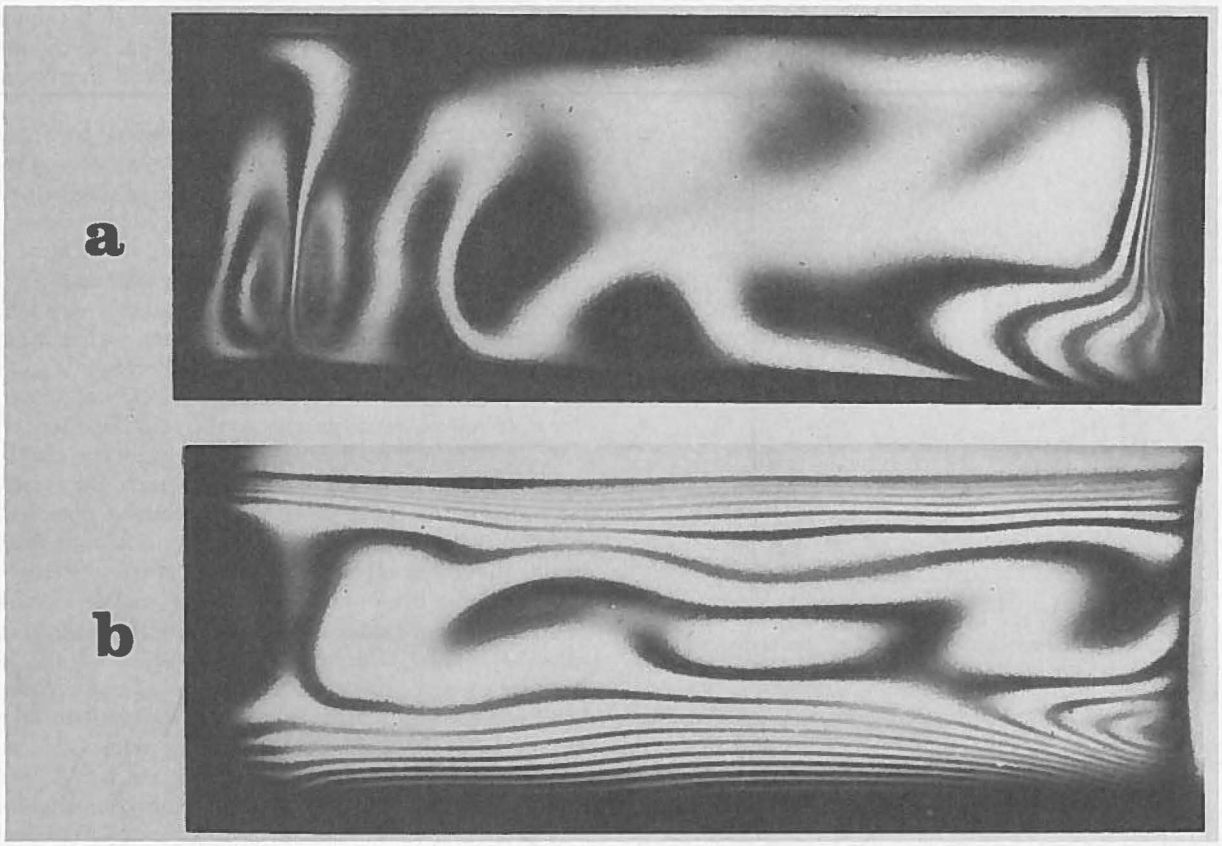

Fig. 11. (*a*) Horizontal and (*b*) vertical isogradient fringes in a wide convection roll showing boundary layer instabilities. Conditions are: $Ra_{vertical} = 67{,}000$, $Ra_{lateral} = 97{,}000$, and $Pr = 1300$. The roll extends from the cold wall on the right to the region on the left-hand side of the field of view marked by characteristic double eyes in the top frame. The pattern within the large roll is time-dependent and the two views were not taken simultaneously. They both show boundary layer instabilities giving rise to ascending thermal plumes in the left half portion of the large roll.

Houseman and McKenzie, 1980] exhibit similar boundary layer instabilities. In this respect, the study of convection with internal heating provides further experimental evidence. There is no lower thermal boundary layer, and the large roll induced by lateral cooling exhibits no small scale uprising plumes. This fact supports the idea that the instabilities seen in the previous case are not generated by mechanical shear within the roll. Instabilities in the upper boundary layer still occur in the case of internal heating. They generate cold downwelling plumes which we have observed by means of the shadowgraph technique.

Figure 14 shows the observed positions and drift velocities of these cold plumes as deduced from a sequence of shadowgraphs. The tank is seen from the top with the cold wall on the right-hand side so that the wide roll covers the right-hand portion bordered by the dashed line. There the cold spots are all drifting toward the cold sidewall, as the large scale circulation carries them away. In the left-hand portion of the tank, white dots also reveal the existence of cold downwelling currents. Their position in space is, however, quite stationary except next to the tank walls. In the previous case with heating from below, the cold upper boundary layer instabilities also occur. Their onset requires a higher Rayleigh number value than for the instabilities in the lower boundary. The critical $Ra_{vertical}$ values for both kinds of instabilities depend upon the lateral Rayleigh number. The actual onset values have not been thoroughly investigated. Results in Figure 13 show that instabilities in the lower boundary layer are observed for a vertical Rayleigh number as low as 3×10^4.

Birth of the large roll. The relevance of the above laboratory experiments for geophysical modeling is critically related with the time required to build up the large roll once lateral cooling begins. For the earth, once a subduction zone starts to operate, the question is, Will the large roll have time to build up before subduction stops? Figure 15 is a plot of the growth of the width of the large roll for three experiments with differ-

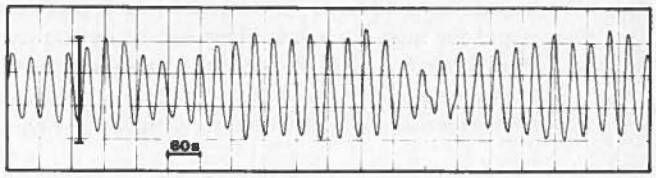

Fig. 12. Strioscopy: time-dependent horizontal deflection of the laser beam after passing through the unstable bottom boundary layer of a large roll similar to that shown in Figure 11. Here the conditions are: $Ra_{vertical} = 88{,}000$, $Ra_{lateral} = 170{,}000$, and $Pr = 440$. The time axis is horizontal, and the vertical bar corresponds to a horizontal temperature gradient equal to $\Delta T_{vertical}/2d$, where d is the depth of the tank and $\Delta T_{vertical}$ amounts to 6.1°C. The laser beam is crossing the bottom boundary layer 0.4 cm above the bottom plate and 4.4 cm away from the cold vertical wall. The width of the large roll is 6.4 cm ($w/d = 3.2$).

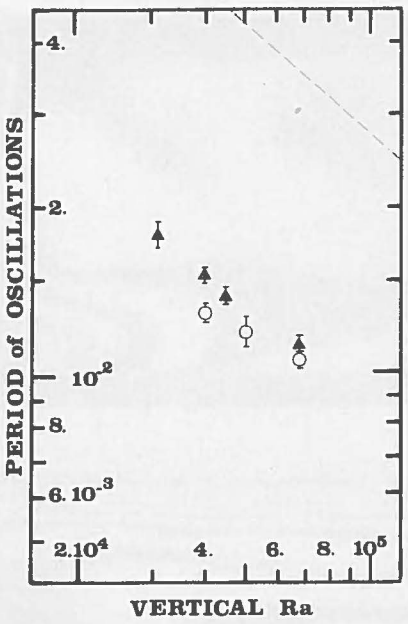

Fig. 13. Period of temperature fluctuations connected with instabilities in the bottom boundary layer of the large roll versus vertical Rayleigh number. The period is given in units of d^2/κ. Triangles are for $Ra_{\text{lateral}} = 67{,}500$, and circles for 100,000. The dashed line corresponds to the results for the Rayleigh-Bénard case in a small box obtained by *Bergé and Dubois* [1979].

ent Rayleigh numbers. At time zero, the cooling fluid is suddenly circulated in the sidewall. The evolution of the convective pattern is observed by differential interferometry. In a first stage, a lateral thermal boundary layer is initiated by heat diffusion, and the cooled material begins to flow down the sidewall. This occurs within a time comparable with the time necessary to thermalize the sidewall. In the next stage, which is clearly seen on the plot, the large roll begins to grow as the cold front propagates rapidly along the bottom of the tank. Preexisting convective structures are swept away. As the upwelling limb of the large roll finally forms, the growth enters a last stage, which is much less rapid than the previous one. It corresponds to an expansion of the large roll as a whole, which implies some rearrangements in the neighboring convective cells. The time scale in the figure is expressed in terms of the time of thermal diffusion through the depth d of the tank. One sees that the creation of the large roll is a relatively rapid phenomenon. It is governed by convective velocities as far as the propagating cold front plays a major role. It is therefore more rapid for high Ra values. This sort of dynamical process is thus faster than the geometrical rearrangement of rolls which is characterized by a phase diffusion velocity [*Pomeau and Manneville,* 1979; *Wesfreid and Croquette,* 1980].

Discussion and Conclusion

This work was undertaken in order to deepen our understanding of the physics of a specific problem: what is the influence of lateral cooling on a convecting fluid layer? This question was first approached with numerical two-dimensional models [*Rabinowicz et al.,* 1980], and it was important to perform a physical test in three dimensions. Furthermore, laboratory experiments were expected to shed some light on time dependent effects. Although the physical richness of the problem became obvious as more experimental results were obtained, the long term objective remains geophysical. It is the understanding of mantle convective processes under the continental lithosphere and the effect of these deep-seated phenomena on tectonic evolution.

The experiments confirm that vigorous lateral cooling organizes the flow next to the cold sidewall into a roll of great lateral extension. They show that two Rayleigh numbers, Ra_{vertical} and Ra_{lateral}, can specify the physical system. In particular the width/depth ratio of the wide roll is function of these numbers but does not depend upon the Prandtl number when the latter has a high value. For low Ra values a very satisfactory check of the numerical models has been performed in the laboratory. For higher Ra values, typically for $Ra_{\text{vertical}} > 3 \times 10^4$, the large scale circulation next to the cold wall is still that of a wide roll with axis parallel to the cold boundary. However, time-dependent smaller scale features are clearly revealed by means of various optical techniques. They consist of hot uprising and cold downwelling plumes generated by boundary layer instabilities. These thermal diapirs are seen drifting in the general circulation of the large roll. Their existence confirms the physical validity of similar instabilities found in two-dimensional numerical models dealing with a somewhat similar large scale circulation [*Lux et al.,* 1979]. This type of small scale circulation contrasts with the longitudinal rolls existing in a sheared convective layer [*Richter and Parsons,* 1975]. Our opinion is that the hot plumes are the preferred small scale mode when a cold return flow is present. The same conclusion has been inferred from numerical modeling [*Kopitzke,* 1979]. Another time-dependent feature demonstrated by the experiments is the rapidity of the growth of the wide roll after lateral cooling has started. The growth time is connected with the penetration of the induced cold front at convective velocities.

Geodynamical speculations related with the formation of a wide roll in the subcontinental upper mantle of the earth next to an oceanic subduction zone lead to the prediction of a variety of observable phenomena. The relevant Rayleigh numbers for the boundary conditions seen in Figure 1 and a mantle viscosity of the order 10^{22}–10^{21} poise amount to 10^5–10^6, Ra_{lateral} being about twice Ra_{vertical}. In this situation, Figure 7 predicts a width/depth ratio for the large roll between 4 and 5. The few runs made with internal heating tend to indicate higher values when heat is not only supplied from below. Rolls extending 3000–4000 km away from the active continental margin can therefore be expected for the earth if one assumes the upper and lower mantles to convect separately.

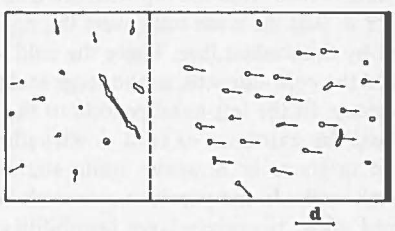

Fig. 14. Position and drift velocity of 'cold spots' in the tank seen in plan view. The fluid is internally heated, and the cold wall is on the right-hand side (thick line). The dashed line indicates the position of the upwelling extremity of the large roll. Conditions are: $T_{\text{top}} = 25°\text{C}$, $T_{\text{lateral}} = 21.5°\text{C}$, $Q = 27\ \text{kW/m}^3$, $Ra_{\text{vertical}}{}^* = 660{,}000$, and $Pr = 210$. The length of each arrow is the displacement observed after 30 s. The length of the bar outside of the rectangle equals the depth of the tank.

This was also inferred from the numerical models [*Rabinowicz et al.,* 1980]. The time necessary to build up this large scale circulation pattern under a continent would be about 200 Ma. Indeed, once subduction has started, the cooled continental mantle material is expected to flow along the base of the upper mantle at a velocity of the order of 2 cm/yr. This duration does not exceed the lifetime of the subduction process in many instances. It has been shown that the geological consequences are far reaching [*Froidevaux and Nataf,* 1981]. For example, the large roll could provide the appropriate mechanism for the breakup of large continental masses like Gondwanaland. Indeed it provides both a mechanical drag underneath the continental lithosphere and a thermal softening of the same lithosphere above the hot uprising limb. Figure 16 shows a map of Gondwana with the position of its active margin. There, subduction is known to have existed for 250 Ma prior to breakup. A wide roll could thus have been formed, with its ascending limb some 4000 km inland. There the Gondwana lithosphere would thin because of the strong heat flux, while the mechanical drag tends to pull the lithosphere toward the active margin. This is roughly what happened when the South Atlantic and Indian Oceans started to open some 135 Ma ago.

Do the boundary layer instabilities observed in the experiments have an equivalent in the earth? It is tempting to associate them with intraplate volcanism, the so-called hot spots. At this stage our main point is that in the earth the small scale convective circulation must also take the form of diapiric motions triggered by boundary layer instabilities. Underneath the subcontinental lithosphere, both cold downwelling and warm upwelling diapirs can form in the top and bottom layers of the wide roll. In this respect, the circulation in the oceanic mantle has a very similar thermal structure at its base. Indeed the plunging lithosphere is still relatively cool as it reaches 700 km. Thus the oceanic return flow also consists of a cold tongue in contact with a hotter lower mantle. Instabilities can be expected at this interface and generate a small scale convection pattern consisting of hot plumes. Of course, the global return flow pattern is not everywhere as simple as sketched in Figure 1 [*Hager and O'Connell,* 1979]. The top boundary layer being the oceanic lithosphere, its high viscosity inhibits the formation of cold sinking diapirs [*Yuen et al.,* 1981]. Small scale bumps observed in the geoid [*McKenzie et al.,* 1980] could reflect the type of small scale circulation proposed here.

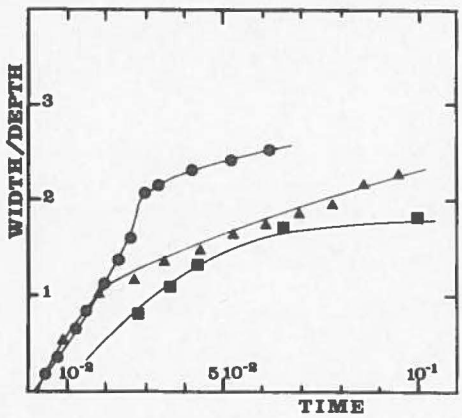

Fig. 15. Growth of the induced large roll: the plot shows the width/depth ratio versus time. The time is given in d^2/κ units, where d is the depth of the tank. Each curve corresponds to a given set of Rayleigh numbers. Circles are for $Ra_{\text{vertical}} = 40{,}000$, $Ra_{\text{lateral}} = 100{,}000$, $Pr = 1300$; triangles for $Ra_{\text{vertical}} = 31{,}000$, $Ra_{\text{lateral}} = 100{,}000$, $Pr = 1300$; and squares for $Ra_{\text{vertical}} = 30{,}000$, $Ra_{\text{lateral}} = 44{,}000$, and $Pr = 3100$.

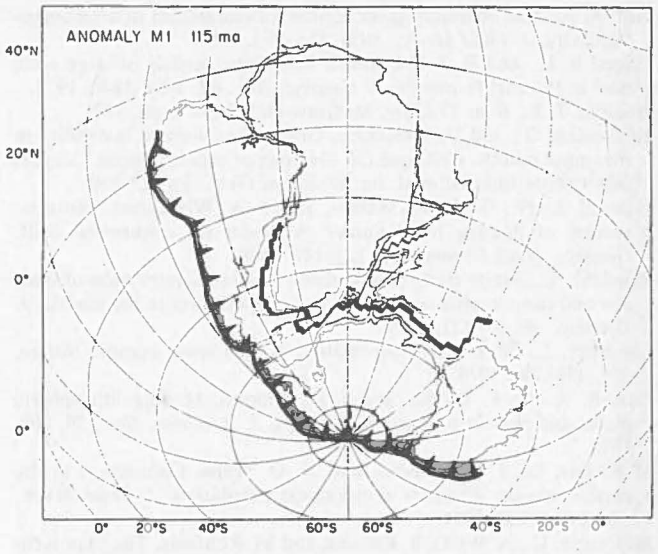

Fig. 16. Map of Gondwanaland 115 Ma ago, just after continental break-up started [redrawn after *Norton and Sclater,* 1979]. The heavy line with triangles idicates the position of the active margin where subduction of oceanic lithosphere took place for some 250 Ma before break-up. The broken line between the continental fragments marks the new plate boundaries formed by the ridges of the South Atlantic and Indian Oceans.

Acknowledgments. We are thankful to M. Françon for lending us his differential interferometer. We also thank P. Bergé and E. Guyon for helpful discussions.

REFERENCES

Allègre, C. J., La géodynamique chimique, *Mém. 4. Ser. Soc. Geol. Fr., 10,* 79–96, 1980.

Bergé, P., and M. Dubois, Study of unsteady convection through simultaneous velocity and interferometric measurements, *J. Phys. Lett., 19,* L.505, 1979.

Bergé, P., and Y. Pomeau, La turbulence, *Recherche, 11,* 422–432, 1980.

Booker, J. R., Thermal convection with strongly temperature-dependent viscosity, *J. Fluid Mech., 4,* 741–754, 1976.

Busse, F. H., and J. A. Whitehead, Oscillatory and collective instabilities in large Prandtl number convection, *J. Fluid Mech., 66*(1), 67–79, 1974.

Chen, M. M., and J. A. Whitehead, Evolution of two dimensional periodic Rayleigh convection cells of arbitrary wave-numbers, *J. Fluid Mech., 31,* 1–15, 1968.

Cormack, D. E., G. P. Stone, and L. G. Leal, The effect of upper surface conditions on convection in a shallow cavity with differentially heated end-walls, *Int. J. Heat Mass Transfer, 18,* 635–648, 1975.

Davies, G. F., Whole mantle convection and plate tectonics, *Geophys. J. R. Astron. Soc., 49,* 459–486, 1977.

De La Cruz, R. S., Asymmetric convection in the upper mantle, *Geofis. Int., 10*(2), 49–56, 1970.

Dubois, M., and P. Bergé, Experimental study of the velocity field in Rayleigh-Bénard convection, *J. Fluid Mech., 85,* 641–653, 1978.

Françon, M., and S. Mallick, *Polarization Interferometers: Applications in Microscopy and Macroscopy,* John Wiley, New York, 1971.

Froidevaux, C., and H. C. Nataf, Continental drift: What driving mechanism?, *Geologische Rundschau,* in press, 1981.

Froidevaux, C., G. Schubert, and D. A. Yuen, Thermal and mechanical structure of the upper mantle: A comparison between continental and oceanic models, *Tectonophysics, 37,* 233–246, 1977.

Gill, A. E., The boundary-layer regime for convection in a rectangular cavity, *J. Fluid Mech., 26*(3), 515–536, 1966.
Hager, B. H., and R. J. O'Connell, Kinematic models of large scale flow in the earth's mantle, *J. Geophys. Res., 84,* 1031–1048, 1979.
Holman, J. P., *Heat Transfer,* McGraw-Hill, New York, 1976.
Houseman, G., and D. McKenzie, Onset of convective instability in the upper mantle, Colloque C4, Geology of oceans, 26ème Congrès Géologique International, Int. Union of Geol., Paris, 1980.
Howard, L. N., W. V. R. Malkus, and J. A. Whitehead, Self-convection of floating heat sources: A model for continental drift, *Geophys. Fluid Dynamics, 1,* 123–142, 1970.
Kopitzke, U., Finite element convection models: Comparison of shallow and deep mantle convection and temperatures in the mantle, *J. Geophys., 46,* 97–121, 1979.
Lliboutry, L., Plate movement relative to rigid lower mantle, *Nature, 250,* 298–300, 1974.
Lux, R. A., G. F. Davies, and J. H. Thomas, Moving lithospheric plates and mantle convection, *Geophys. J. R. Astron. Soc., 58,* 209, 1979.
McKenzie, D., J. M. Roberts, and N. O. Weiss, Convection in the earth's mantle: Towards a numerical simulation, *J. Fluid Mech., 62*(3), 465–538, 1974.
McKenzie, D., A. Watts, B. Parsons, and M. Roufosse, The plan form of mantle convection beneath the Pacific Ocean, *Nature, 288,* 442–446, 1980.
Merzkirch, W., *Flow Visualization,* Academic, New York, 1974.
Norton, I. O., and J. G. Sclater, A model for the evolution of the Indian Ocean and the break-up of Gondwanaland, *J. Geophys. Res., 84,* 6803–6830, 1979.
Oertel, H., Jr., and K. Bühler, A special differential interferometer used for heat convection investigations, *Int. J. Heat Mass Transfer, 21,* 1111–1115, 1978.
Pomeau, Y., and P. Manneville, Stability and fluctuation of a spatially periodic convective flow, *J. Phys. Lett., 40,* 609–612, 1979.
Rabinowicz, M., Convection dans le manteau, Cas des plaques lithosphériques bordées par une zone de subduction; confrontation des résultats de la modélisation numérique avec les données géophysiques, Thèse Univ. de Pris XI, Orsay, 1980.
Rabinowicz, M., B. Lago, and C. Froidevaux, Thermal transfer between the continental asthenosphere and the oceanic subducting lithosphere: Its effect on subcontinental convection, *J. Geophys. Res., 85,* 1839–1853, 1980.
Richter, F. M., Experiments on the stability of convection rolls in fluids whose viscosity depends on temperature, *J. Fluid Mech., 89*(3), 553–560, 1978.
Richter, F. M., Focal mechanisms and seismic energy release of deep and intermediate earthquakes in the Tonga-Kermadec region and their bearing on the depth extent of mantle flow, *J. Geophys. Res., 84,* 6783–6795, 1979.
Richter, F. M., and B. Parsons, On the interaction of two scales of convection in the mantle, *J. Geophys. Res., 80,* 2529–2541, 1975.
Roberts, P. H., Convection in horizontal layers with internal heat generation, *J. Fluid Mech., 30,* 33–49, 1967.
Schubert, G., D. A. Yuen, and D. L. Turcotte, Role of phase transitions in a dynamic mantle, *Geophys. J. R. Astron. Soc., 42,* 705–735, 1975.
Schwiderski, E. W., and H. J. A. Schwab, Convection experiments with electrolytically heated fluid layers, *J. Fluid Mech., 48,* 703–719, 1971.
Sung, C. M., and R. G. Burns, Kinetics of the olivine spinel transition: Implication in deep-focus earthquake genesis, *Earth Planet. Sci. Lett., 32,* 165, 1976.
Torrance, K. E., and D. L. Turcotte, Structure of convection cells in the mantle, *J. Geophys. Res., 76,* 1154–1161, 1971.
Tritton, D. J., and M. N. Zarraga, Convection in horizontal layers with internal heat generation, *J. Fluid Mech., 30,* 21–31, 1967.
Vening Meinesz, F. A., *Thermal Convection in the earth's Mantle, Continental Drift,* edited by S. K. Runcorn, pp. 145–176, Academic, New York, 1962.
Wesfreid, J. E., and V. Croquette, Forced phase diffusion in Rayleigh-Bénard convection, *Phys. Rev. Lett., 45*(8), 634–637, 1980.
Yuen, D. A., W. R. Peltier, and G. Schubert, On the existence of a second scale of convection in the upper mantle, *Geophys. J. R. Astron. Soc., 65,* 171–190, 1981.

(Received November 17, 1980;
revised February 19, 1981;
accepted February 24, 1981.)